Sensors and Actuators B 258 (2018) 566–573

Contents lists available at ScienceDirect

Sensors and Actuators B: Chemical

journal homepage: www.elsevier.com/locate/snb

Surface-imprinted SiO_2@Ag nanoparticles for the selective detection of BPA using surface enhanced Raman scattering

Wenmin Yin [1], Long Wu [1], Fan Ding, Qin Li, Pan Wang, Jinjie Li, Zhicheng Lu, Heyou Han *

State Key Laboratory of Agricultural Microbiology, College of Food Science and Technology, College of Science, Huazhong Agricultural University, Wuhan, 430070, PR China

ARTICLE INFO

Article history:
Received 14 May 2017
Received in revised form
21 November 2017
Accepted 22 November 2017
Available online 23 November 2017

Keywords:
Surface enhanced Raman scattering
Molecular imprinting
Bisphenol A
SiO_2@Ag nanoparticles
Food safety analysis

ABSTRACT

To circumvent the limitations of natural antibodies, receptor, or enzyme, molecular imprinting technique has received intensive attention in analytical methods Herein, based on surface enhanced Raman scattering (SERS) molecularly imprinted polymer (SERS-MIP), a SERS-MIP sensor has been developed for the sensitive and selective detection of bisphenol A (BPA). To construct the BPA sensor, raspberry-type SiO_2@Ag nanoparticles (SiO_2@Ag NPs) were prepared to act as supporting substrate, and BPA was adopted as template molecule, tetraethyl orthosilicate (TEOS) as functional monomer and 3-aminopropyltriethoxysilane (APTES) as cross-linker. Due to the strong plasma resonance character of Ag NPs, the SERS-MIP sensor showed good sensitivity in the detection of BPA. The core-shell and satellite-like structure of the SiO_2@Ag composites could provide a large surface area for BPA recognition by molecular binding domains. In addition, the sensor could prevent interferences such as 4,4′-(Hexafluoroisopropylidene) diphenol (BPAF) and 4,4′-Dihydroxybiphenyl (DOD). Moreover, the real water samples were tested to verify the reliability and feasibility of the method. Under the optimal conditions, the proposed method behaved good analytical performance to BPA with a wide linear range from 1.75×10^{-11} to 1.75×10^{-6} M and a detection limit of 1.46×10^{-11} M.

1. Introduction

Recently, people have been paying great attention on food safety as the food safety problem becomes increasingly prominent. For example, illegal abuse of food packing has brought serious hazards to the ecological environment and human health in many food safety problems [1,2]. Bisphenol A (BPA), an important industrial chemical, has been widely applied in polycarbonate plastics, epoxy resins, food packing and many other products [3–5]. However, it is inevitable that BPA can release from many plastic packages, such as nursing bottles, plastic water bottles and sealant, leading to food and environmental pollution [6]. Meanwhile, related studies have shown that BPA is a kind of endocrine disruptor and excessive intake will potentially interfere with the endocrine system of wildlife and humans, do harm to liver and renal function, lower immune function, and even increase the risk of cancer [7–9]. Thus, the use of BPA, especially in feeding bottles was strictly regulated in many countries for the sake of human health [10,11]. In this regard, it is of great significance and highly desired to develop specific and sensitive analytical methods for the detection of BPA.

As is well known, various analytical methods have been applied in BPA detection such as high-performance liquid chromatography (HPLC), gas chromatography-mass spectrometry (GC–MS), enzyme-linked immunosorbent assay (ELISA) and some other analytical tools [12–14], for example, fluorescent, optical, colorimetric and electrochemical sensors [15–18]. However, though some of these analytical techniques are widely used with good precision, their applications are seriously restricted due to the complicated and professional operation procedures, high cost and relative low sensitivity. The other methods are simple, fast response and easy operation, but the accuracy and selectivity of those techniques cannot meet the needs of actual sample detection. Due to the excellent sensitivity, fast response, rich molecular information and nondestructive data acquisition, SERS is extensively used from biological analysis to environment monitoring and food safety, even clinical diagnosis and therapy [19,20]. Thus, it can be a very attractive method for BPA determination using SERS technique. For example, by using pyridine functionalized silver nanoparticles as SERS substrates, a recent paper was reported for the detection of BPA with the semi-quantitative detection ranging from 0.25 to 20 $\mu g\,L^{-1}$ [21]. Furthermore, it was reported that the oestrogen molecules

* Corresponding author.
E-mail address: hyhan@mail.hzau.edu.cn (H. Han).
[1] Equal contribution.

https://doi.org/10.1016/j.snb.2017.11.141
0925-4005/

Table 1
Comparison of the proposed method with other methods for BPA detection.

Detection technique	Liner range (M)	LOD (M)	References
Optical sensor	10^{-10}—4×10^{-9}	2×10^{-11}	[16]
Colorimetric method	1.5×10^{-7}—6.1×10^{-7}	4.8×10^{-10}	[17]
Multiplexed SERS	2.2×10^{-7}—4.38×10^{-6}	8.8×10^{-8}	[21]
SERS	4×10^{-11}—4×10^{-10}	1.7×10^{-11}	[26]
MIRF sensor	10^{-7}—2.5×10^{-6}	2.9×10^{-8}	[35]
Voltammetric sensor	5×10^{-8}—10^{-5}	8×10^{-9}	[44]
PE sensor	3.5×10^{-7}—1.4×10^{-5}	1.14×10^{-7}	[45]
Aptamer SERS	1.3×10^{-11}—1.3×10^{-9}	1.3×10^{-11}	[46]
SERS MIP	1.75×10^{-11}—1.75×10^{-6}	1.46×10^{-11}	This work

MIRF: molecularly imprinted ratiometric fluorescent; PE: photoelectrochemical.

including BPA showed very weak affinity with the metal surface [22], which largely restrains the SERS detection of BPA. To address this problem, many research methods have been developed by combining SERS with separation processing [23] or selectivity techniques [24,25]. For example, Chung et al. designed a SERS sensor for BPA detection by using double strand DNA-embedded Au/Ag core-shell nanoparticles as substrates, which showed a detection limit of 10 fM [25]. Feng et al. proposed a SERS-encoded strategy via gold nanoparticle-nanorod heteroassemblies for BPA detection, which behaved a wide liner range from 0.001 to 1 ng mL^{-1} with the detection limit of 3.9 pg mL^{-1} [26]. However, the interferences in the real samples could have great influence on the SERS performance such as detection sensitivity and selectivity. Thus, it is crucial and meaningful to develop a new SERS method with highly selective for BPA detection.

Owing to their advantages such as high loading capacities, efficient affinity to target molecules, sufficient selectivity and stability, easy design of recognition sites and low production cost, molecularly imprinted polymers (MIPs) have become a competitive tool in the field of molecular recognition, food sample preparation and biosensors [27,28]. Many methods have been developed to synthesize MIPs, and non-covalent imprinting is widely used through the interaction between the functional monomer and templates [29,30]. Here, strategies for non-covalent imprinting include core-shell imprinting, precipitation polymerization, solid-phase imprinting, bulk polymerization and mini emulsion polymerization [31,32]. Because they can provide a deal of effective imprinting sites to rebind the template molecules, core-shell spherical MIPs have been intensively used when coupled with many other techniques [33,34]. For example, Lu et al. put forward a facile strategy to prepare ratiometric fluorescence molecularly imprinted sensor for the sensitive detection of BPA with detection limit of 29 nM [35]. Tan et al. developed a novel electrochemical sensor based on molecularly imprinted polypyrrole/graphene quantum dots composites, which could specifically recognize BPA in aqueous solution and water samples [36]. Inspired by that, it could be a promising idea to combine MIPs with SERS for the selective and sensitive detection of BPA (Table 1).

In this work, a new SERS biosensor was developed for highly sensitive and selective detection of BPA based on molecularly imprinted SiO_2@Ag NPs composites (MIP-ir-SiO_2@Ag NPs) (Scheme 1). In the SERS system, the core/shell composites (SiO_2 nanospheres as core and Ag NPs as shell) were acted as supporting substrates. It was demonstrated that the core-satellite nanostructure could provide plasmonic enhancement by plasmon resonance between silver particles and shell layer [37,38]. Thus, the signal could be greatly enhanced by using the core-satellite SiO_2@Ag NPs as MIPs supporting substrates. Considering this, TEOS was adopted as functional monomer, APTES as cross-linker, and the target molecule BPA as template molecule to prepare BPA printed template (Scheme 1). After that, BPA were removed by a simple washing process, and MIP-ir-SiO_2@Ag NPs behaved good recombining ability and specificity to BPA. Moreover, the performance of MIP-ir-SiO_2@Ag NPs towards BPA and their application to practical samples were investigated, which revealed that the proposed SERS-MIP method could be applied to the selective and sensitive detection of BPA in water samples.

2. .Materials and methods

2.1. Chemicals and materials

Bisphenol A (BPA), 4,4′-Dihydroxybiphenyl (DOD), tetraethyl orthosilicate (TEOS, 99%), 4,4′-(Hexafluoroisopropylidene) diphenol (BPAF), and (3-aminopropyl) triethoxysilane (APTES, 97%) were purchased from Aladdin. Polyvinyl pyrrolidone (PVP) was purchased from Sigma-Aldrich. Silver nitrate ($AgNO_3$), ammonium hyroxide ($NH_3{\cdot}H_2O$, AR) and other relevant reagents were bought from Sinopharm Chemical Reagent Co., Ltd. Unless otherwise mentioned, ultrapure water acquired from a Millipore water purification system (Milli-Q, Millipore, 18.2 MΩ resistivity) and was used throughout the experiment.

2.2. Instrumentation

SERS measurements were carried out using a Raman spectrometer (Renishaw, U.K.) equipped with a confocal microscope (Leica, Germany). The band of a silica wafer at 520 cm^{-1} was used to calibrate spectrometer. The SERS spectra were acquired under a He-Ne laser (633 nm) with a laser power of 10 mW, and 10 s exposure with one accumulation. Spectral manipulation such as baseline adjustment and smoothing were performed using the NGSLabSpec5 software package.

2.3. Preparation of SiO_2@Ag nanospheres

The preparation procedures of SiO_2@Ag nanospheres were illustrated in Scheme 1. According to our previous work [39], SiO_2 nanospheres (nearly 300 nm) were first synthesized and then mixed with $Ag(NH_3)_2OH$ to prepare SiO_2@Ag nanospheres. The details are described in Supporting Information.

2.4. Preparation of BPA-imprinted SiO_2@Ag nanospheres

The BPA imprinted-removed materials (MIP-ir-SiO_2@Ag NPs) were prepared by non-covalent imprinting method. The none imprinted materials (NIP-ir-SiO_2@Ag NPs) were synthesized with the same procedures. The preparation procedures are all described in Supporting Information.

2.5. Detection methods

Prior to the SERS measurements, MIP-ir-SiO_2@Ag NPs and NIP-ir-SiO_2@Ag NPs were incubated with different concentrations of BPA, respectively. After that, the filter paper (0.5 mm) was soaked with the above polymer composites. Next, the filter paper was placed on the injector and washed with water to remove the free BPA. Finally, the filter paper was taken out and kept at room temperature till drying. The obtained filter paper was interrogated with the Raman microscope.

2.6. Selectivity studies

To estimate the selectivity of MIP-ir-SiO_2@Ag NPs, 100 μL of BPA, BPAF and DOD was mixed with 100 μL MIP-ir-SiO_2@Ag NPs, respectively. The mixture was shaken in a 1.5 mL centrifuge tube

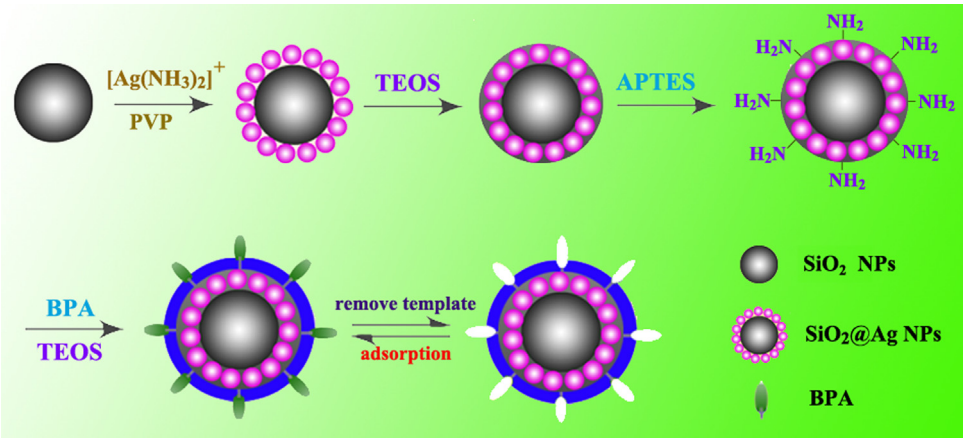

Scheme 1. Illustration of the synthetic route for the surface-imprinted SiO_2@Ag NPs nanocomposites.

at 4 °C for 6 h. The final solution was centrifuged to remove the supernatant and the precipitate was dispersed for Raman tests.

2.7. Treatment of real samples

The MIP-ir-SiO_2@Ag NPs was applied in the detection of BPA in lake water, tap water and pure milk, respectively. Lake water was collected from the South Lake (located in Huazhong Agricultural University) and then filtered with a 0.22 μm filter head. The tap water was collected from the laboratory and used without further pretreatment. The pure milk was purchased from local market. The extraction procedures for milk sample are described in Supporting Information. A 100 μL aliquot of the above samples was analyzed by the Raman spectroscopy.

3. Results and discussion

3.1. Characterization of BPA-imprinted SiO_2@Ag nanospheres

The UV–vis and FT-IR absorption spectra were first adopted to characterize the MIP-ir-SiO_2@Ag NPs and NIP-ir-SiO_2@Ag NPs. The formation of SiO_2@Ag NPs was firstly characterized by UV–vis (Fig. S1A). The strong and broad peak around 450 nm indicates the formation of Ag NPs on the surface of SiO_2 nanospheres, which revealed that SiO_2@Ag nanospheres were successfully synthesized. Following that, MIP-ir-SiO_2@Ag NPs were prepared for the specific recognition with BPA. As shown in Fig. 1A, BPA molecule behaved two strong characteristic absorption peaks located at 228 nm and 279 nm (curve d), which were consistent with the $\pi \rightarrow \pi^*$ transitions of aromatic C=C bond. Compared with MIP- ir-SiO_2@Ag NPs and NIP-ir-SiO_2@Ag NPs, the MIP-BPA-SiO_2@Ag NPs still remained the characteristic peak at 279 nm (curve a). However, after removing BPA with methanol and acetic acid mixture solution, the characteristic peak was disappeared (curve b and c), which suggested the successful preparation of MIP-BPA-SiO_2@Ag NPs.

To further verify the performance of MIP-ir-SiO_2@Ag NPs combining with BPA, the related materials were characterized by FT-IR spectroscopy (Fig. 1B). BPA (curve d) and MIP-BPA-SiO_2@AgNPs (curve a) showed characteristic peak at 1611 cm^{-1} and 1598 cm^{-1} (C=C stretch), 1300 cm^{-1} (C–O vibration), 2964 cm^{-1} and 3068 cm^{-1} (C–H vibration), revealing the successful recognition of MIP-ir-SiO_2@AgNPs with BPA. Moreover, a characteristic peak at 790 cm^{-1} (Si-O vibration) appeared in all the SiO_2 based materials: MIP-ir-SiO_2@Ag NPs (curve b), NIP-ir-SiO_2@Ag NPs (curve c), and MIP-BPA-SiO_2@Ag NPs (curve a), which revealed that the MIP was coated on the surface of the SiO_2@Ag NPs. The absorbance band around 1540 cm^{-1} (N–H band) suggested the

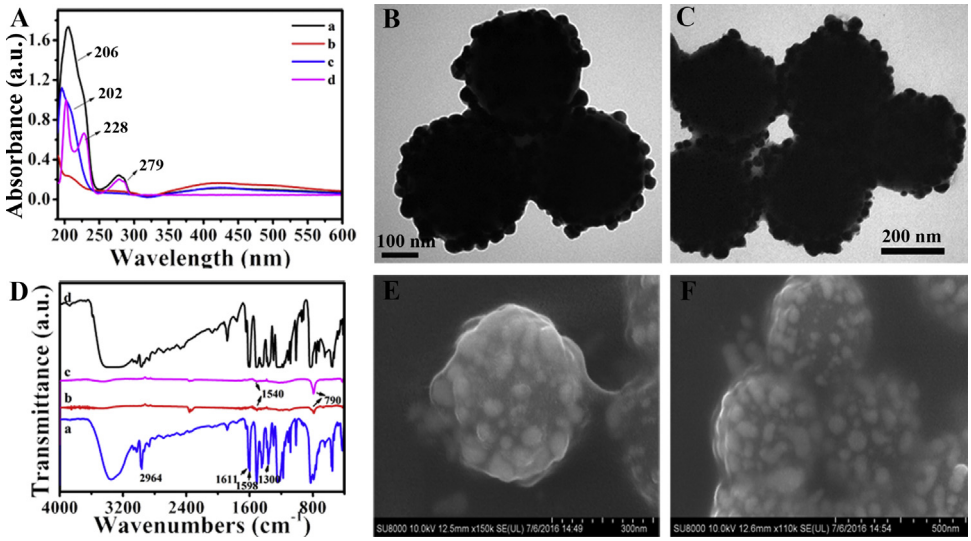

Fig. 1. (A) UV–vis absorption and (D) FT-IR spectra of MIP-BPA-SiO_2@Ag NPs (a), MIP-ir-SiO_2@Ag NPs (b), NIP-ir-SiO_2@Ag NPs (c) and BPA (d). TEM images of (B) SiO_2@Ag NPs and (C) MIP-ir-SiO_2@Ag NPs. SEM images of MIP-ir-SiO_2@Ag NPs at different magnification (E) and (F).

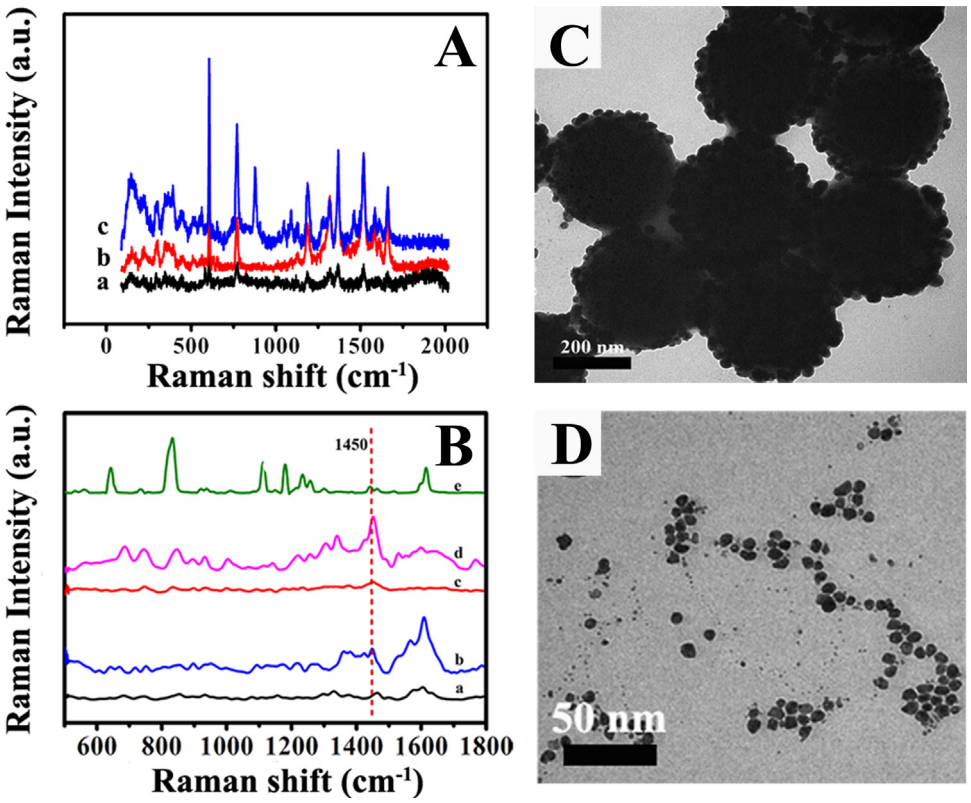

Fig. 2. (A) Raman spectra of BPA on different SERS substrates (a: none-SERS substrate; b: Ag NPs; c: SiO_2@Ag NPs). (B) Raman spectra of (a) NIP-ir-SiO_2@Ag NPs; (b) MIP-ir-SiO_2@Ag; (e) BPA solid; SERS spectrum of (c) NIP-ir-SiO_2@Ag NPs and (d) MIP-ir-SiO_2@Ag NPs after incubating with 1.75×10^{-6} M BPA solution in a mixture of water and methanol (1:1, v/v), respectively. TEM images of SiO_2@Ag NPs (C) and Ag NPs (D).

existence of aminopropyl group in the SiO_2 based materials. All the results showed that the MIP was successfully grafted on the surface of SiO_2@Ag NPs.

The performance of the MIP-ir-SiO_2@Ag NPs was also evaluated by CV and EIS. In the presence and absence of SERS-MIP substrate, the differences appear in the current (CV) and electron-transfer resistance (Ret). In comparison, the current of SiO_2@Ag NPs modified electrode is lower than that of bare electrode, mainly due to the low electrical conductivity of silica (Fig. S2A). When SiO_2@Ag NPs were further coated with MIP layer, the current was considerably decreased, which was consistent with the results of EIS. Fig. S2B exhibited the conductivity of bare GCE, SiO_2@Ag NPs/GCE and MIP-ir-SiO_2@Ag NPs/GCE, which was presented by the semicircle of EIS plot. The charge transfer resistance (R_{et}) values of bare GCE and SiO_2@Ag NPs/GCE were 62 Ω and 150 Ω, respectively. After the molecular film was imprinted on the surface of SiO_2@Ag NPs, the R_{et} value further increased to 373 Ω, which can be ascribed to the poor conductivity of polymer. The above mentioned experimental data fitted well with the Randles circuit model (Fig. S2B inset). The results suggested that the polymer was successfully imprinted on the surface of SiO_2@Ag NPs.

As depicted in Fig. 1, TEM images of SiO_2@Ag NPs and MIP-ir-SiO_2@Ag NPs showed numerous Ag NPs on the silica surface, which could provide excellent SERS enhancement when compared with the pure SiO_2 nanospheres due to the plasmon resonance effect of Ag NPs (Fig. S1B). Compared with SiO_2@Ag NPs (Fig. 1B), the MIP-ir-SiO_2@Ag NPs (Fig. 1C, E and F) have a SiO_2@Ag NPs core with a diameter of ~300 nm and a thin MIP shell with the thickness of ~10 nm, which could exhibit better water solubility and specificity.

3.2. SERS activity of BPA on MIP-ir-SiO_2@Ag NPs

To verify the SERS activity of MIP-ir-SiO_2@Ag NPs, the SERS measurements on Ag NPs, SiO_2@Ag NPs, MIP-ir-SiO_2@Ag NPs and NIP-ir-SiO_2@Ag NPs were studied, respectively. As shown in Fig. 2A, SiO_2@Ag NPs (curve c) behaved stronger SERS enhancement when compared with bare Ag NPs (curve b) and non-SERS substrate (curve a), which can be attributed to the advantage of numerous hotspots and binding sites for probing molecules on SiO_2@Ag NPs. From the morphology of SiO_2@Ag NPs (Fig. 2C) and Ag NPs (Fig. 2D), it can deduce that three-dimensional (3D) silver substrates offer better SERS enhancement than Ag NPs, which was consistent with previous reports [40,41]. Meanwhile, as shown in Fig. 2B, the MIP-ir-SiO_2@Ag NPs (curve d) exhibited strong characteristic SERS bands around 685 cm^{-1}, 745 cm^{-1}, 845 cm^{-1}, 1000 cm^{-1}, 1450 cm^{-1} and 1770 cm^{-1}, which was consistent with the fact that MIP-ir-SiO_2@AgNPs and BPA formed the intermolecular hydrogen bond via the interaction between amine groups and phenolic hydroxyl groups. However, only the bands at 845 cm^{-1} and 1450 cm^{-1} are consistent with the Raman spectrum of solid BPA (curve e), and the band at 1450 cm^{-1} exhibited stronger Raman intensity. Therefore, the SERS shift at 1450 cm^{-1} could be used to identify the presence of BPA in MIP-ir-SiO_2@Ag NPs for its characteristic fingerprint Raman band. Furthermore, no obvious SERS signal (1450 cm^{-1}) was observed in MIP-ir-SiO_2@Ag NPs (curve a), NIP-ir-SiO_2@Ag NPs (curve b) and NIP-ir-SiO_2@Ag NPs incubated with BPA (curve c), which indicated that the recognition between the MIP-ir-SiO_2@Ag NPs and target molecules was through the amine groups and phenolic hydroxyl groups but not the physical adsorption.

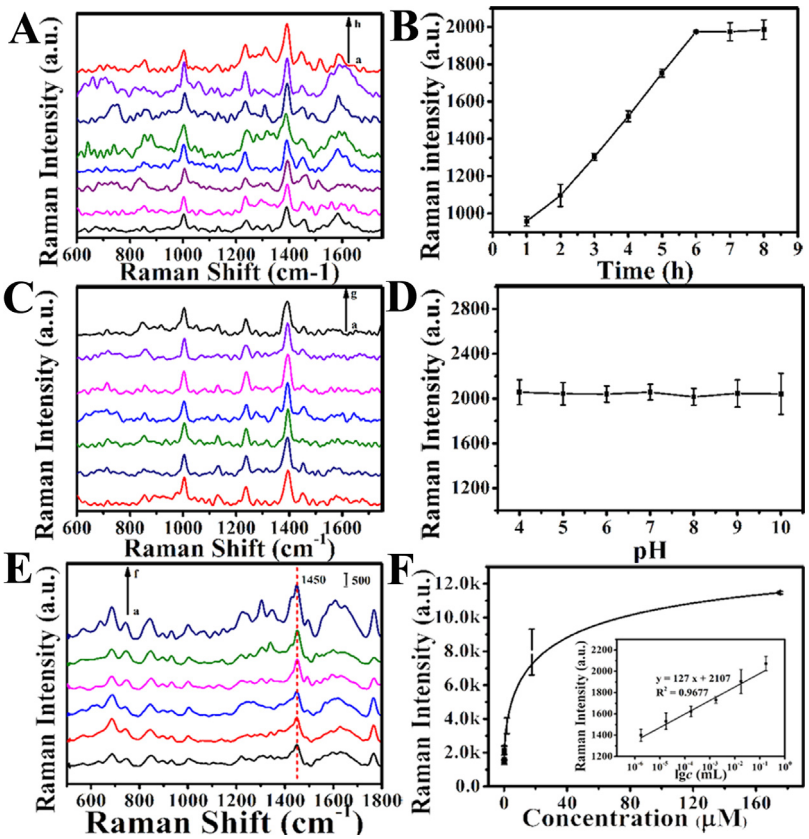

Fig. 3. (A) Influence of the incubation time (from a to h: 1–8 h) on the SERS spectra of MIP-ir-SiO_2@Ag NPs in BPA solution (1.75×10^{-6} M). (B) The plots of SERS intensity versus incubation time from 1 to 8 h at 1450 cm^{-1}. (C) Influence of the solution pH (from a to g: 4, 5, 6, 7, 8, 9, 10) on the SERS spectra of MIP-ir-SiO_2@Ag NPs in BPA solution (1.75×10^{-6} M). (D) The plots of SERS intensity versus solution pH from 4 to 10 for the bands at 1450 cm^{-1}. (E) SERS spectra of MIP-ir-SiO_2@Ag NPs incubated with different concentrations of BPA solution (from a to f: 1.75×10^{-11} to 1.75×10^{-6} M). (F) Plots of intensity versus BPA concentrations corresponding to (E) at 1450 cm^{-1} based on MIP-ir-SiO_2@Ag NPs (The inset shows the liner relationship between the SERS intensity and the concentration of BPA within the range from 1.75×10^{-11} to 1.75×10^{-6} M). The error bars represent the average standard deviations with three SERS tests.

3.3. Optimization of the experimental conditions

Different influence factors were carefully investigated to obtain the optimal experimental conditions. Firstly, incubating time was investigated from 1 h to 8 h. As shown in Fig. 3A and B, as the incubating time increased, the Raman intensity of the band at 1450 cm^{-1} increased accordingly. But after 6 h, it can be seen clearly that the Raman intensity tended to be balanced, which revealed that the binding sites on the MIP-ir-SiO_2@Ag NPs dominated by the BPA molecules were saturated. Hence, the optimal incubating time was adopted as 6 h in the following experiments.

It was reported that pH can not only change the charge of BPA molecules but also the net charge of the $-(CH_2)_3NH_2$ group, having an impact on the formation of the intermolecular hydrogen bonding between the amine group and phenolic hydroxyl group [24,42]. In the lower pH range, $-(CH_2)_3NH_2$ was easily protonated and generated $-(CH_2)_3NH_3^+$, while at a high pH value, the BPA molecules were more easily deprotonated and then weakened the hydrogen bonding between the amine group and phenolic hydroxyl group [24]. But as shown in Fig. 3C and D, it is obvious that the pH of the mixed solution has no influence to the SERS intensity of the BPA molecules, which can be ascribed to the constant methanol content (50%) of the solution [43]. Therefore, the pH of the mixed solution had no obvious influence on the Raman intensity, which provides great convenience in the detection of real samples.

3.4. Quantitative detection of BPA using MIP-ir-SiO_2@Ag NPs

Under the above optimized experimental conditions, the SERS spectra of BPA at different concentrations were measured on MIP-ir-SiO_2@Ag NPs. As shown in Fig. 3E, the intensity of the fingerprint Raman band of BPA at 1450 cm^{-1} increased with the increment of BPA concentrations. Fig. 3F presents the plots of SERS intensity versus the concentration of BPA at 1450 cm^{-1}. A linear relationship between SERS intensity and the BPA concentration was demonstrated with the range of 1.75×10^{-11} to 1.75×10^{-6} M. The results can be put as the following equation: $y = 2107 + 127 \lg c$ ($R^2 = 0.9677$), where y is the Raman peak intensity at 1450 cm^{-1} and c is the concentration of target molecules BPA. The detection limit of MIP-ir-SiO_2@Ag NPs for BPA was estimated to be 1.46×10^{-11} M (S/N = 3). The high sensitivity of MIP-ir-SiO_2@Ag NPs for BPA could be ascribed to the recognition cavities in the thin shells on the surface of SiO_2@Ag nanospheres, which offered functional groups combining with BPA molecules and exclusive sites for BPA molecules approaching to Ag NPs surface. Nevertheless, for NIP-ir-SiO_2@Ag NPs, as shown in Fig. S3, even when the BPA concentration was 1.75×10^{-6} M, the band at 1450 cm^{-1} is weak and no characteristic band of BPA could be observed, which revealed that the interaction force between the NIP-ir-SiO_2@Ag NPs and BPA is non-specific adsorption and can be easily washed away by the mixed solution of methanol and acetic acid. The lower signal fluctuation, higher sensitivity and R value of the SERS results verify the superiority of the proposed SERS-MIP detection method.

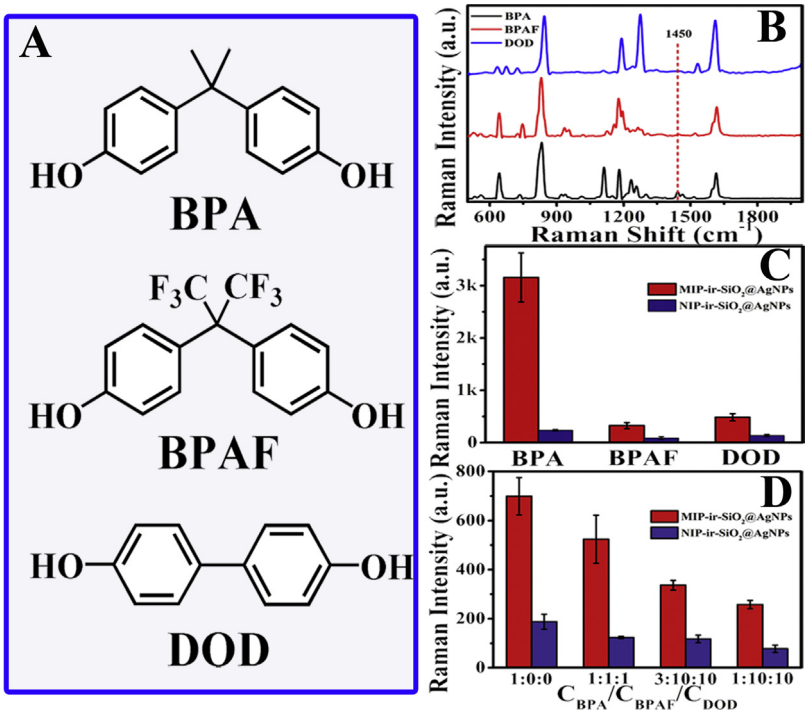

Fig. 4. (A) Chemical structures of BPA and the structural analogues (BPAF and DOD). (B) Raman spectra of BPA, BPAF and DOD solid. (C) The SERS intensity depends on the band at 1450 cm^{-1} for MIP-ir-SiO_2@Ag NPs and NIP-ir-SiO_2@Ag NPs after incubating with 1.75×10^{-7} M of BPA, BPAF and DOD. (D) Verification of the selectivity of MIP-ir-SiO_2@Ag NPs and MIP-ir-SiO_2@Ag NPs for BPA (0.058 μM) in the presence of different concentration ratios of $C_{BPA}/C_{BPAF}/C_{DOD}$ (1:0:0, 1:1:1, 3:10:10 and 1:10:10). The error bars represent the average standard deviations with three tests.

3.5. Selectivity of the MIP-ir-SiO_2@Ag NPs

To further evaluate the selectivity of the MIP-ir-SiO_2@Ag NPs, two BPA structural analogues BPAF and DOD, as shown in Fig. 4A, were chosen as control under the same experimental conditions. The Raman spectra of the three kinds of solid samples are exhibited in Fig. 4B. It is obvious that no SERS band around 1450 cm^{-1} was observed in the spectra of BPAF or DOD solid sample, which illustrated that it is reasonable to choose the band at 1450 cm^{-1} for quantitative analysis. As depicted in Fig. 4C, MIP-ir-SiO_2@Ag NPs exhibited much higher sensitivity towards BPA than that of NIP-ir-SiO_2@Ag NPs. However, when used for the detection of BPAF or DOD, both of them show no obvious signal response. The results indicated that MIP-ir-SiO_2@Ag NPs has the highest SERS signal in the presence of BPA, which revealed its good selectivity.

Also, the selectivity was confirmed by discussing the BPA SERS intensity when MIP-ir-SiO_2@Ag NPs were incubated in different concentrations of BPA/BPAF/DOD. As shown in Fig. 4C, the SERS intensity of BPA at 1450 cm^{-1} decreased slightly with same concentration of BPAF and DOD. However, when the MIP-ir-SiO_2@Ag NPs were incubated in the pooled solution with a ratio of 1:10:10 for competitive binding (Fig. 4D), the SERS intensity decreased to 36.86% as compared with the relative intensity in BPA solution (1:0:0). Meanwhile, for the NIP-ir-SiO_2@Ag NPs, the SERS relative intensity of BPA was only decreased to 58.79% (1:10:10) when compared with that in BPA solution (1:0:0), revealing that the NIP-ir-SiO_2@Ag NPs have stronger nonspecific adsorption than MIP-ir-SiO_2@Ag NPs. All the results showed that the BPA imprinted MIP-ir-SiO_2@Ag NPs behaved high selectivity and affinity for BPA because of the template-specific sites.

3.6. Determination of BPA in real samples

To investigate the practicality of the developed method, MIP-ir-SiO_2@Ag NPs were applied to the measurements of BPA in real samples. In this study, three kinds of samples (south lake water, tap water and pure milk) were discussed. Considering that the pH had no obvious influence on the BPA detection, so the real samples were tested without adjusting pH before SERS detection. The SERS results showed that no BPA signal was observed when the MIP-ir-SiO_2@Ag NPs were incubated in the three samples, which revealed that there was no BPA included in the samples. To verify the potential utility of the proposed method for real samples, the three real samples were spiked with the same concentration of BPA (1.75×10^{-9} M). As shown in Table S1, the concentration of BPA in the tap water, south lake water and pure milk were consistent with the added concentrations with quantitative recoveries of 89.98%, 101.31% and 97.58%, indicating that MIP-ir-SiO_2@Ag NPs has good accuracy and it is acceptable for food sample analysis.

4. Conclusion

In this work, a novel core-shell SiO_2@Ag NPs MIP composites were synthesized by using SiO_2@Ag NPs as supporting substrate, BPA as template molecule, TEOS as functional monomer and APTES as cross-linker. The synthesized MIP-ir-SiO_2@Ag NPs was satellite-like and uniform with a diameter of about 300 nm with a silica shell of about 10 nm thickness. Due to the strong plasma resonance character of the Ag NPs and high selectivity feature of the MIPs, MIP-ir-SiO_2@Ag NPs exhibited highly sensitive and selective to the detection of BPA molecules. Under the optimal conditions, the proposed method behaved good analytical performance to BPA with a wide linear range from 1.75×10^{-11} to 1.75×10^{-6} M and a detection limit of 1.46×10^{-11} M. Meanwhile, MIP-ir-SiO_2@Ag NPs exhibited good selectivity towards BPA different from 4,4′-Dihydroxybiphenyl (DOD) and 4,4′-(Hexafluoroisopropylidene) diphenol (BPAF). Additionally, the SERS-MIP displayed good precision with the recovery of 89.98–111.31% in the real sample

detection, suggesting its potential application in food testing, environmental monitoring and bioassay.

Acknowledgements

We gratefully acknowledge the financial support from National Key R & D Program (2016YFD0500700), National Natural Science Foundation of China (21375043, 21175051) and Scitech Innovation Foundation of Huazhong Agriculture University (2662017PY042). We thank Heng Yan for the help at Hubei Provincial Institute for Food Supervision and Test.

Appendix A. Supplementary data

Supplementary data associated with this article can be found, in the online version, at https://doi.org/10.1016/j.snb.2017.11.141.

References

[1] L. Wu, K. Chen, Z. Lv, T. Li, K. Shao, F. Shao, H. Han, Hydrogen-bonding recognition-induced aggregation of gold nanoparticles for the detection of the migration of melamine monomers using dynamic light scattering, Anal. Chim. Acta 845 (2014) 92–97.
[2] L. Wu, W. Yin, K. Tang, D. Li, K. Shao, Y. Zuo, J. Ma, J. Liu, H. Han, Enzymatic biosensor of horseradish peroxidase immobilized on Au-Pt nanotube/Au-graphene for the simultaneous determination of antioxidants, Anal. Chim. Acta 933 (2016) 89–96.
[3] X. Zhang, L. Wu, J. Zhou, X. Zhang, J. Chen, A new ratiometric electrochemical sensor for sensitive detection of bisphenol A based on poly-β-cyclodextrin/electroreduced graphene modified glassy carbon electrode, J. Electroanal. Chem. 742 (2015) 97–103.
[4] R. Shen, W. Zhang, Y. Yuan, G. He, H. Chen, Electrochemical detection of bisphenol A at graphene/melamine nanoparticle-modified glassy carbon electrode, J. Appl. Electrochem. 45 (2015) 343–352.
[5] P. Yu, Y. Liu, X. Zhang, J. Zhou, E. Xiong, X. Li, J. Chen, A novel electrochemical aptasensor for bisphenol A based on triple-signaling strategy, Biosens. Bioelelctron. 79 (2016) 22–28.
[6] P. Jing, X. Zhang, Z. Wu, L. Bao, Y. Xu, C. Liang, W. Cao, Electrochemical sensing of bisphenol A by graphene-1-butyl-3-methylimidazolium hexafluorophosphate modified electrode, Talanta 141 (2015) 41–46.
[7] I.A. Lang, T.S. Galloway, A. Scarlett, Association of urinary bisphenol a concentratioin with medical disorders and laboratory abnormalities in adults, JAMA 141 (2015) 41–46.
[8] A.M. Soto, C. Sonnenschein, Environmental causes of cancer: endocrine disruptors as carcinogens, Nat. Rev. Endocrinol. 6 (2010) 363–370.
[9] X. Wang, X. Lu, L. Wu, J. Chen, 3D metal-organic framework as highly efficient biosensing platform for ultrasensitive and rapid detection of bisphenol A, Biosens. Bioelectron. 65 (2015) 295–301.
[10] Y. Wan, K. Choi, S. Kim, K. Ji, H. Chang, S. Wiseman, P.D. Jones, J.S. Khim, S. Park, J. Park, M.H.W. Lam, J.P. Giesy, Hydroxylated polybrominated diphenyl ethers and bisphenol a in pregnant women and their matching fetuses: placental transfer and potential risks, Environ. Sci. Technol. 44 (2010) 5233–5239.
[11] L. Wu, D. Deng, J. Jin, X. Lu, J. Chen, Nanographene-based tyrosinase biosensor for rapid detection of bisphenol A, Biosens. Bioelectron. 35 (2012) 193–199.
[12] C. Lin, M. Fuh, S. Huang, Application of liquid-liquid–liquid microextraction and high-performance liquid chromatography for the determination of alkylphenols and bisphenol-A in water, J. Sep. Sci. 34 (2011) 428–435.
[13] A.R. Fontana, M.M.D. Toro, J.C. Altamirano, One-Step derivatization and preconcentration microextraction technique for determination of bisphenol a in beverage samples by gas chromatography-Mass spectrometry, J. Agric. Food Chem. 59 (2011) 3559–3563.
[14] I. Kubo, T. Kanamatsu, S. Furutani, Microfluidic device for enzyme-linked immunosorbent assay (ELISA) and its application to biophenol a sensing, Sens. Mater. 26 (2014) 615–621.
[15] P. Gallo, I.D.M. Pisciottano, F. Esposito, E. Fasano, G. Scognamiglio, G.D. Mita, T. Cirillo, Determination of BPA, BPB BPF, BADGE and BFDGE in canned energy drinks by molecularly imprinted polymer cleaning up and UPLC with fluorescence detection, Food Chem. 220 (2017) 406–412.
[16] Y. Ma, J. Liu, H. Li, Diamond-based electrochemical aptasensor realizing a femtomolar detection limit of bisphenol A, Biosens. Bioelectron. 92 (2017) 21–25.
[17] J. Xu, Y. Li, J. Bie, W. Jiang, J. Guo, Y. Luo, F. Shen, C. Sun, Colorimetric method for determination of bisphenol A based on aptamer-mediated aggregation of posotively charged gold nanoparticles, Microchim. Acta. 182 (2015) 2131–2138.
[18] Y. Ma, F. You, K. Promthaveepong, N. Li, Ultrasensitive Biophenol A sensing based on responsive plasmonic nanoparticles, Sens. Actuators B Chem 245 (2017) 369–374.
[19] P. Wang, L. Wu, Z. Lu, Q. Li, W. Yin, F. Ding, H. Han, Gecko-inspired nanotentacle surface-Enhanced raman spectroscopy substrate for samling and reliable detection of pesticide residues in fruits and vegetables, Anal. Chem. 89 (2017) 2424–2431.
[20] Y. Wang, Z. Yu, W. Ji, Y. Tanaka, H. Sui, B. Zhao, Y. Ozaki, Enantioselective discrimination of alcohols by hydrogen bonding: a SERS study, Angew. Chem. Int. Ed. 126 (2014) 14086–14090.
[21] C.D. Bleye, E. Dumont, C. Hubert, P.Y. Sacré, L. Netchacovitch, P.F. Chavez, P. Hubert, E. Ziemons, A simple approach for ultrasensitive detection of bisphenols by multiplexed surface-enhanced Raman scattering, Anal. Chim. Acta 888 (2015) 118–125.
[22] X. Han, P. Pienpinijtham, B. Zhao, Y. Ozaki, Coupling reaction-based ultrasensitive detection of phenolic estrogens using surface-enhanced resonance raman scattering, Anal. Chem. 83 (2011) 8582–8588.
[23] R.M. Connatser, M. Cochran, R.J. Harrison, M.J. Sepaniak, Analytical optimization of nanocomposite surface enhanced Raman spectroscopy/scattering detection in microfluidic separation devices, Electrophoresis 29 (2008) 1441–1450.
[24] J. Xue, D. Li, L. Qu, Y. Long, Surface-imprinted core-shell Au nanoparticles for selective detection of bisphenol A based on surface-enhanced Raman scattering, Anal. Chim. Acta 777 (2013) 57–62.
[25] E. Chung, J. Jeon, J. Yu, C. Lee, J. Choo, Surface-enhanced Raman scattering aptasensor for ultrasensitive trace analysis of bisphenol A, Biosens. Bioelectron. 64 (2015) 560–565.
[26] J. Feng, L. Xu, G. Cui, X. Wu, W. Ma, H. Kuang, C. Xu, Building SERS-active heteroassemblies for ultrasensitive biophenol a detection, Biosens. Bioelectron. 81 (2016) 138–142.
[27] J. Ashley, M.A. Shahbazi, K. Kant, V.A. Chidambara, A. Wolff, D.D. Bang, Y. Sun, Molecularly imprinted polymers for sample preparation and biosnsing in food analysis: progress and perspectives, Biosens. Bioelectron. 91 (2017) 606–615.
[28] E. Mazzotta, A. Turco, I. Chianella, A. Guerreiro, S.A. Piletsky, C. Malitesta, Solid-phase synthesis of electroactive nanoparticles of molecularly imprinted polymers. A novel platform for indirect electrochemical sensing applications, Sens. Actuator B Chem. 229 (2016) 174–190.
[29] K. Puzio, R. Delépée, R. Vidal, L.A. Agrofoglio, Combination of computational methods: adsorption isotherms and selectivity tests for the conception of a mixed non-covalent-semi-covalent molecularly imprinted polymer of vanillin, Anal. Chim. Acta 790 (2013) 47–55.
[30] M. Dabrowski, P.S. Sharma, Z. Iskierko, K. Noworyta, M. Cieplak, W. Lisowski, S. Oborska, A. Kuhn, W. Kutner, Early diagnosis of fungal infections using piezomicrogravimetric and electric chemosensors based on polymers molecularly imprinted with D–arabitol, Biosens. Bioelectron. 79 (2016) 627–635.
[31] X. Song, S. Xu, L. Chen, Y. Wei, H. Xiong, Recent advances in molecularly imprinted polymers in food analysis, J. Appl. Polym. Sci. 131 (2014) 40766.
[32] F. Canfarotta, A. Poma, A. Guerreiro, S. Piletsky, Solid-phase synthesis of molecularly imprinted nanoparticles, Nat. Protoc. 11 (2016) 443–455.
[33] S. Han, X. Li, Y. Wang, C. Su, A core-shell Fe_3O_4 nanoparticle-CdTe quantum dot-molecularly imprinted polymer composite for recognition and seperation of 4-nonylphenol, Anal. Meth. 6 (2014) 2855–2861.
[34] R.J. Uzuriaga-Sánchez, S. Khan, A. Wong, G. Picasso, M.I. Pividori, M.D.P.T. Sotomayor, Magnetically separable polymer (Mag-MIP) for selective analysis of biotin in food samples, Food Chem. 190 (2016) 460–467.
[35] H. Lu, S. Xu, Visualizing BPA by molecularly imprinted ratiometric fluorescence sensor based on dual emission nanoparticles, Biosens. Bioelectron. 92 (2017) 147–153.
[36] F. Tan, L. Cong, X. Li, Q. Zhao, H. Zhao, X. Quan, J. Chen, An electrochemical sensor based on molecularly imprinted polypyrrole/graphene quantum dots composite for detection of bisphenol A in water samples, Sens. Actuators B Chem. 233 (2016) 599–606.
[37] I. Pastoriza-Santos, D. Gomez, J. Pérez-Juste, L.M. Liz-Marzán, P. Mulvaney, Optical properties of metal nanoparticle coated silica spheres: a simple effective medium approach, Phys. Chem. Chem. Phys. 6 (2004) 5056–5060.
[38] E.R. Encina, E.A. Coronado, On the far optical properties of Ag-Au nanosphere pairs, J. Phys. Chem. C 114 (2010) 16278–16284.
[39] L. Wu, W. Yin, K. Tang, K. Shao, Q. Li, P. Wang, Y. Zuo, X. Lei, Z. Lu, H. Han, Highly sensitive enzyme-free immunosorbent assay for porcine circovirus type 2 antibody using Au-Pt/SiO2 nanocomposites as labels, Biosens. Bioelectron. 82 (2016) 177–184.
[40] R. Kodiyath, T.A. Papadopoulos, J. Wang, Z.A. Combs, H. Li, R.J.C. Brown, J.L. Brédas, V.V. Tsukruk, Silver-Decorated cylindrical nanopores: combining the third dimension with chemical enhancement for efficient trace chemical detection with SERS, J. Phys. Chem. C 116 (2012) 13917–13927.
[41] F. Shao, Z. Lu, C. Liu, H. Han, K. Chen, W. Li, Q. He, H. Peng, J. Chen, Hierarchical nanogaps within bioscaffold arrays as a high-Performance SERS substrate for animal virus biosensing, ACS Appl. Mater. Inter. 6 (2014) 6281–6289.
[42] D. Gao, Z. Zhang, M. Wu, C. Xie, G. Guan, D. Wang, A surface functional monomer-Directing strategy for highly dense imprinting of TNT at silica nanoparticles, J. Am. Chem. Soc. 129 (2007) 7859–7866.
[43] A.G. Gonázlea, D. Rosales, J.L. Gómez-Ariza, Solvent effects on the dissociation of aliphatic carboxylic acids in water—N,N-dimethylformamide mixtures, Anal. Chim. Acta 228 (1990) 301–306.
[44] B. Su, H. Shao, N. Li, X. Chen, Z. Cai, X. Chen, A sensitive bisphenol A voltammetric sensor relying on AuPd nanoparticles/graphene composites modified glassy carbon electrode, Talanta 166 (2017) 126–132.
[45] L. Xu, P. Yan, H. Li, S. Ling, J. Xia, Q. Xu, J. Qiu, H. Li, Photoelectrochemical sensing of bisphenol a based on graphitic carbon nitride/bismuth oxyiodine composites, RSC Adv. 7 (2017) 7929–7935.

[46] H.L. Marks, M.V. Pishko, G.W. Jackon, G.L. Coté, Rational design of a bisphenol a aptamer selective surface-Enhanced raman scattering nanoprobe, Anal. Chem. 86 (2014) 11614–11619.

Biographies

Wenmin Yin was born in Jiangxi Province, China, in 1993. She received his BS degree Huazhong Agricultural University in 2015. Her research interests focus on the preparation of surface enhanced Raman scattering (SERS) substrate and their applications.

Long Wu was born in Hubei Province, China, in 1988. He is now a PhD in the School of Food Science and Technology at the Huazhong Agricultural University under the direction of Professor Heyou Han. His research interests focus on biosensing and bioanalysis.

Fan Ding was born in Hubei Province, China, in 1994. He received his BS degree Huazhong Agricultural University in 2016. His research interests focus on biosensing and bioanalysis.

Qin Li was born in Hubei Province, China, in 1992. She received his BS degree Huazhong Agricultural University in 2014. Her research interests focus on synthesis and modification of plasmonic nanostructures for biosensing.

Pan Wang was born in Hubei Province, China, in 1991. He received his BS degree in Tarim University in 2014. His research interests focus on the preparation of surface enhanced Raman scattering (SERS) substrate and their applications.

Jinjie Li was born in Hebei Province, China, in 1990. He received his master degree in 2015 in Tianjin University of Commerce. His research interests focus on the preparation of surface enhanced Raman scattering (SERS) substrate and their applications.

Zhicheng Lu received his Ph.D degree in 2008 in Jilin University. He was a post doctor in Suzhou Institute of Nano-Tech and Nano-Bionic and Huazhong Agricultural University, consecutively. He is now working at Huazhong Agricultural University. His scientific interests focus on synthesis and modification of plasmonic nanostructures for biosensing.

Heyou Han was born in Anhui Province, China, in 1962. He received his Ph.D. degree in Wuhan University in 2000 and he was a postdoctor in Jeckson State University (America) from 2000 to 2004. He has been a Professor of Huazhong Agricultural University since 2004. He has published over 100 papers in international journals. His research interests focus on functionalized nanomaterials for bioanalysis, food safety and energy applications.